Research article **Open Access**

Douglas J. Little* and Deb M. Kane

Investigating the transverse optical structure of spider silk micro-fibers using quantitative optical microscopy

DOI 10.1515/nanoph-2016-0125
Received July 11, 2016; accepted September 15, 2016

Abstract: The transverse optical structure of two orb-weaver (family *Araneidae*) spider dragline silks was investigated using a variant of the inverse-scattering technique. Immersing the silks in a closely refractive index-matched liquid, the minimum achievable image contrast was greater than expected for an optically homogeneous silk, given what is currently known about the optical absorption of these silks. This "excess contrast" indicated the presence of transverse optical structure within the spider silk. Applying electromagnetic scattering theory to a transparent double cylinder, the minimum achievable irradiance contrast for the *Plebs eburnus* and *Argiope keyserlingi* dragline silks was determined to be consistent with step index refractive index contrasts of $1–4\times10^{-4}$ and $6–7\times10^{-4}$, respectively, supposing outer-layer thicknesses consistent with previous TEM studies (50 nm and 100 nm, respectively). The possibility of graded index refractive index contrasts within the spider silks is also discussed. This is the strongest evidence, to date, that there is a refractive index contrast associated with the layered morphology of spider silks and/or variation of proportion of nanocrystalline components within the spider silk structure. The method is more generally applicable to optical micro-fibers, including those with refractive index variations on a sub-wavelength scale.

Keywords: spider silk; micro-fibers; refractive index; quantitative microscopy; optical scattering.

***Corresponding author: Douglas J. Little,** MQ Photonics Research Centre, Department of Physics and Astronomy, Macquarie University, North Ryde, Sydney, NSW 2109, Australia, e-mail: douglas.little@mq.edu.au
Deb M. Kane: MQ Photonics Research Centre, Department of Physics and Astronomy, Macquarie University, North Ryde, Sydney, NSW 2109, Australia

1 Introduction

Silk is emerging as a promising new class of photonic materials. Silk is a protein-based nanocomposite with a well-known capacity to respond structurally to its chemical environment, such as pH and water content [1, 2]. Silk is also a very stable material that forms at room temperature, enabling complex biomolecules to be incorporated into the silk matrix [3]. Silk-based materials are, therefore, very promising candidates for optically based chemical and biological sensors that are biocompatible, biodegradable, and highly sensitive. Silk-based photonic devices fabricated, to date, have mostly involved working with silk fibroin solution cast into planar photonic structures such as diffraction gratings [4]. There is emerging interest now in employing silks' intrinsic chemical response for micro-fiber-based sensor geometries.

Spider silks from orb-weaver spiders are naturally suited to this application, as they possess the required optical and geometric properties; they are optically transparent, spun as micro-fibers (with diameters typically between 0.5 and 5.0 μm), with a double-cylinder structure, and are produced naturally by spiders with no further post-processing requirements. Spider silks have also been proposed as interconnects between integrated photonic components [5], taking advantage of silks' well-known mechanical robustness [6].

To date, much is unknown about the transverse optical (refractive index) structure of spider silks. Transmission electron microscopy has previously revealed the presence of layers within the silks, with this layered structure being more pronounced in some species than others [7, 8]. It is also possible that the nanocrystalline domains within the silks' nanocomposite structure are not spread uniformly throughout the silk, but may vary radially within the central core of the silk. These structural elements could potentially manifest as discrete or graded refractive index layers. In addition to affecting the light-guiding properties of spider silks, transverse optical structure is a potential proxy for studying the distribution

of the silks' nanocrystalline domain elements and other mechanical qualities.

To probe the optical structure of spider silks, a variant of the inverse-scattering technique; where analysis of scattered electromagnetic fields are used to infer the properties of the scatterer, was employed. The experiment was contained within a standard bright-field microscope, which was used to illuminate the silk and image the scattered fields. Silks were immersed in a liquid with a traceable calibrated refractive index to maximize the sensitivity of the scattered field to the silks' optical properties. Dragline silks are birefringent double cylinders, with the birefringent axis oriented parallel to the silk axis, and so rotating the incident linear polarization effectively "tunes" the refractive index of the silk. This effect has previously been utilized to measure the principal refractive indices of these birefringent silks [9].

The analytical procedure presented in this paper is based on the key observation that, even with careful index matching, the silks cannot be rendered completely invisible; there is always a "residual" visibility (or contrast) that emerges, due to a) the mixing of p- and s-polarized scattered fields, which possess slightly different transverse profiles, b) mismatch in the imaginary refractive index (or optical absorption), and c) transverse optical structure in the silks. The electromagnetic scattering theory can then be used to link the observed residual visibility to the optical characteristics of the silks, enabling the measurement of the principal refractive indices, the optical absorption (if the cylinder is assumed to be optically homogeneous), and the detection of transverse optical structure (when the absorption is independently determined). This procedure can be applied, in principle, at any wavelength where the silk and immersion liquid are transparent.

Section 2 of this paper outlines the theoretical basis of this analytical approach in detail. The procedure for calculating the optical properties of spider silks from images of the scattered field at different polarizations is outlined, as well as the procedure used to evaluate uncertainties. Section 3 details the experimental implementation in the specific case of dragline silks from *Plebs eburnus* and *Argiope keyserlingi*. Measurement of the silks' optical properties is presented in Section 4, assuming a homogeneous silk. The strong contradiction between the calculated optical absorption of the silk with existing measurements is held as evidence that a transverse optical structure is almost certainly present within these silks. Quantitative analysis of the internal refractive index contrast is also presented for step index and graded index refractive index profiles. The main conclusions of this work are presented in Section 5.

2 Measuring the optical properties of silk: theory and uncertainties

The analytical approach used in this paper is designed for application to uniaxial birefringent cylinders in a double-cylinder configuration, with the birefringent axis lying parallel to the silk axis. The double-cylinder configuration arises naturally from the silk-spinning process, where two spinnerets each yield a single cylinder, which then adhere together. The principal refractive indices of the double cylinder are labeled;

$$\mathbf{n_p} = n_p - i\kappa_p, \tag{1}$$

$$\mathbf{n_s} = n_s - i\kappa_s, \tag{2}$$

where $\mathbf{n_p}$ and $\mathbf{n_s}$ are the complex refractive indices for light polarized parallel and perpendicular to the birefringent axis, respectively. If the double cylinders are homogeneous, full characterization of the refractive indices requires evaluation of four quantities: n_p, n_s, κ_p, and κ_s. As silks generally do not exhibit any obvious linear dichroism, the optical absorption is assumed to be isotropic, hence,

$$\kappa_p = \kappa_s = \kappa. \tag{3}$$

As with all immersion-based analysis techniques, double cylinders are immersed in a liquid with refractive index $\mathbf{n_L} = n_L - i\kappa_L$ such that $n_s < n_L < n_p$. As the double cylinders' refractive index at some polarization orientation, θ, is given by

$$n(\theta) = \frac{\cos^2\theta}{n_p^2} + \frac{\sin^2\theta}{n_s^2}, \tag{4}$$

there exists a polarization orientation, θ_0, such that $n(\theta_0) = n_L$.

The double cylinder was positioned a distance z_0 behind the focal (object) plane of the imaging objective, where z_0 was defined as the position that yielded the highest irradiance contrast when imaging the scattered field with a parallel-polarized incident field at normal incidence. Modeled scattered fields on the X–Y plane intersecting the z-position where the on-axis irradiance was highest, could then be directly compared with experimental images and circumvent the need to accurately measure the position of the double cylinder with respect to the focal plane.

Silks were then imaged at both p- and s-polarizations. The visibility of the double cylinder under illumination was quantified by three contrast parameters, C_p, C_s, and C_0, defined as

$$C_p = I_{\max} / I_0 \quad (\theta = 0), \tag{5}$$

$$C_s = I_{\min} / I_0 \quad (\theta = \pi/2), \tag{6}$$

$$C_0 = I_{\min} / I_0 \quad (\theta = \theta_0), \tag{7}$$

where $I_{\max}$ and $I_{\min}$ denote the maximum and minimum irradiances, respectively, in the measured irradiance profiles, and I_0 is the incident (or background) irradiance. Uncertainties in C_p, C_s, and C_0 (labeled δC_p, δC_s, and δC_0) were calculated as twice the standard deviation of the normalized irradiance.

As the polarizations are separable in the case of a cylindrical scatterer, the theoretical relationship between normalized irradiance in the object volume (I_p, I_s) and the optical properties of the double cylinder can be summarized as

$$I_i = \int f_i(\mathbf{n_i}, \mathbf{n_L}, \mathbf{k}, a) d\mathbf{k}, \tag{8}$$

where $i = p, s$; a is the radii of each cylinder in the double-cylinder structure, and $\mathbf{k}$ is the incident wave vector. The functions f_p and f_s are derived from electromagnetic scattering theory [10, 11]. It was assumed, based on previous TEM studies of spider dragline silk, that the double cylinders were in contact, with the same radius and refractive index, and with both cylinder axes in a plane parallel to the focal plane of the imaging objective.

To obtain a similar relation for the irradiance in the image volume, the functions f_p and f_s were convolved with the point-spread function of the imaging objective, p.

$$I_i' = \int p * f_i(\mathbf{n_i}, \mathbf{n_L}, \mathbf{k}, a) d\mathbf{k} = F_i(\mathbf{n_i}, \mathbf{n_L}, \mathbf{k}', a) \tag{9}$$

where the prime denotes the image volume, $*$ denotes a 2-D convolution, and $\mathbf{k}'$ denotes the central illumination wave vector. F_i represents the same thing as f_i, except with the numerical aperture of the incident field and imaging objective accounted for. As the double cylinder is closely refractive index matched with the surrounding medium, and $\mathbf{k}'$ is usually fixed normal to the focal plane with magnitude defined by the measurement wavelength, Eq. (9) can be approximated as

$$I_i' \approx F_i(\Delta n_i, \Delta\kappa, a), \tag{10}$$

where $\Delta n_i = n_i - n_L$ and $\Delta\kappa = \kappa - \kappa_L$ $(i = p, s)$.

Optical properties of double cylinders were inferred by determining the optical constants that minimized the following error terms:

$$\Delta C_p = |\max(I_p') - C_p| \tag{11}$$

$$\Delta C_s = |\min(I_s') - C_s| \tag{12}$$

$$\Delta C_0 = |\min(I_p' \cos^2\theta_0 + I_s' \sin^2\theta_0) - C_0|, \tag{13}$$

where max and min denote the maximum and minimum values in the specified quantities. While the irradiance is imaged over a 2-D plane, the symmetry of the scatterer means that the profile can be reduced to a 1-D cross-section.

To minimize the error terms, ΔC_p and ΔC_s were optimized for several estimates of κ. As the remaining value of ΔC_0 was approximately linear with κ, new estimates for κ that simultaneously minimized all three error terms could be computed reasonably quickly with a Newton's method-type approach.

Uncertainties in n_p, n_s, and κ were derived by linearizing f_p and f_s about the measured values for these quantities. For brevity, perfect positive correlation was assumed (yielding the largest uncertainty estimates).

$$\delta\Delta\kappa \left|\frac{\partial C_0}{\partial \Delta\kappa}\right| = \delta C_0 + \delta a \left|\frac{\partial C_0}{\partial a}\right| \tag{14}$$

$$\delta\Delta n_p \left|\frac{\partial C_p}{\partial n_p}\right| = \delta C_p + \delta\Delta\kappa \left|\frac{\partial C_p}{\partial \Delta\kappa}\right| + \delta a \left|\frac{\partial C_p}{\partial a}\right| \tag{15}$$

$$\delta\Delta n_s \left|\frac{\partial C_s}{\partial n_s}\right| = \delta C_s + \delta\Delta\kappa \left|\frac{\partial C_s}{\partial \Delta\kappa}\right| + \delta a \left|\frac{\partial C_s}{\partial a}\right|, \tag{16}$$

where $\delta\Delta n_p$, $\delta\Delta n_s$, and $\delta\Delta\kappa$ represent uncertainties in Δn_p, Δn_s, and $\Delta\kappa$, respectively. Partial derivatives in Eq. (14) were computed numerically in the process of optimizing the error terms using the procedure outlined above. Given the optical properties of the double cylinder and liquid are uncorrelated, the final uncertainties for n_p, n_s, and κ were calculated as

$$(\delta n_p)^2 = (\delta n_L)^2 + (\delta\Delta n_p)^2 \tag{17}$$

$$(\delta n_s)^2 = (\delta n_L)^2 + (\delta\Delta n_s)^2 \tag{18}$$

$$(\delta\kappa)^2 = (\delta\kappa_L)^2 + (\delta\Delta\kappa)^2, \tag{19}$$

where δn_L and $\delta\kappa_L$ represent uncertainties in n_L and κ_L, respectively, and were determined using specifications provided by the manufacturer of the refractive index liquid.

3 Experimental procedure

3.1 Sample collection and preparation

Spider silk samples were collected from the orb webs of two orb-web spider species, *Plebs eburnus* and *Argiope*

keyserlingi. Spiders were collected from the grounds of Macquarie University (North Ryde, Sydney, Australia) and housed in a laboratory with controlled temperature, humidity, and day-night cycle. Spiders were watered each day and fed *Drosophila* (fruit) flies three to four times a week. Dragline silks were collected from webs using small Perspex frames backed with double-sided sticky tape, which helped preserve the native strain of the silk. A second layer of tape was then used to secure the silk and also acted as a spacer that enabled the silk to be suspended about 100 μm above a microscope coverslip when imaging.

3.2 Microscope system and image acquisition

An Olympus IX-81 inverted microscope (Tokyo, Japan) was used to image the silks. The instrument was operated in transmission mode, using a 40× objective (NA = 0.6). Silks were aligned so that the plane containing the axes of both cylinders in the double cylinder structure were oriented parallel to the image plane of the microscope (Figure 1). The metal-halide (Olympus U-PS50MH) illumination source was filtered using an aperture stop set to minimum,

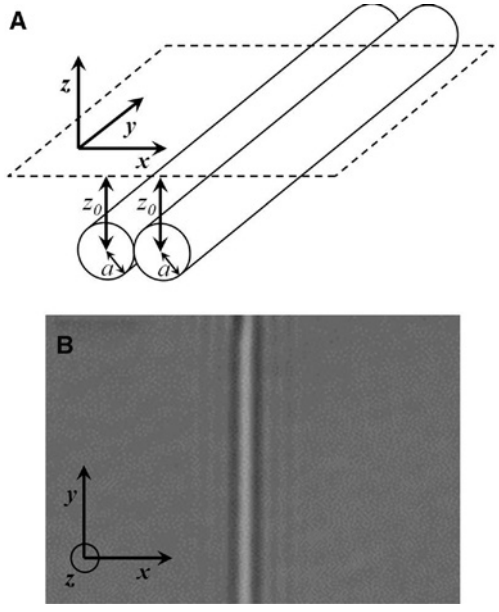

Figure 1: (A) Orientation of the double cylinders with respect to the object plane of the microscope (dashed line). The incident central wave vector, **k′**, is in the $+z$ direction, and *p* and *s* polarizations are oriented in the *y*- and *x*-directions, respectively. (B) Sample image of a silk double cylinder (defocused by an amount, z_0), depicting the orientation of the Cartesian axes. Images are integrated along the *y*-direction to obtain irradiance profiles along the *x*-direction.

corresponding to a numerical aperture of around 0.06. The bandwidth of the wavelength filters used to filter the incident illumination was around 10 nm. Filters with center wavelengths 450 nm, 486 nm, 546 nm, 589 nm, and 656 nm were used to investigate wavelength dependence.

Irradiance profiles at the image plane were recorded using an Olympus DP-72 digital camera. Images were collected as 8-bit grayscale and were averaged over 64 acquisitions to minimize random temporal noise. Because the background illumination field was not completely uniform, a background subtraction was performed using the formula;

$$I_{bc} = I + \bar{I}(1 - I_b / \bar{I}_b) \tag{20}$$

where I_{bc} represents the background-corrected image, I and $\bar{I}$ represent the original image and its average grayscale level, respectively, and I_b and $\bar{I}_b$ represent the background image (i.e. with the spider silk removed) and its mean grayscale level, respectively. Performing the background subtraction in this way ensured that the correct contrast values were preserved through the operation.

After background subtraction, images were then normalized to the background level (i.e. the grayscale level far from the silk). Silks were oriented vertically in the field of view of the camera, which enabled a 20- to 30-fold reduction in random spatial noise by averaging the grayscale levels along the length of the silk to obtain a 1-D irradiance profile along the cross-section of the silk.

3.3 Silk immersion

Silks were immersed in a NIST traceable refractive index liquid from Cargille (Cedar Grove, NJ, USA). The condition that n_L lays between n_p and n_s was checked by rotating the illumination polarization orientation through 90°. If this condition was satisfied, the irradiance profile would undergo a characteristic "inversion" (Figure 2).

Liquids were temperature calibrated to the ambient temperature using the known thermo-optic coefficient. Liquids were wavelength calibrated using dispersion data supplied by Cargille. The imaginary refractive index of the liquid, κ_L, was calculated using;

$$\kappa_L = \frac{\alpha}{2k_0} \tag{21}$$

where α is the absorption coefficient supplied by Cargille. Uncertainty in the real component of the refractive index was specified as ± 0.0002 at 589 nm, and ± 0.001 at 486 nm and 656 nm. Uncertainties at other wavelengths were inferred using a Monte Carlo approach in conjunction

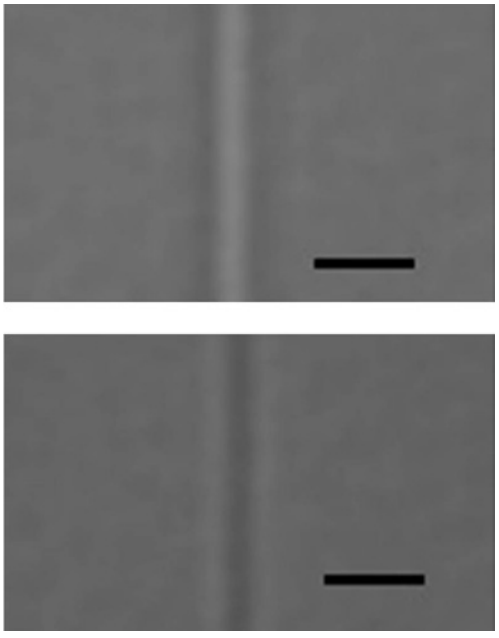

Figure 2: Defocused images of an immersed silk double cylinder with *p*- (top) and *s*-polarized (bottom) illumination. The observed inversion in the contrast demonstrates that, in this instance, n_L is between n_p and n_s. The scale bar is 5 μm.

with the Hartmann dispersion formulae [12], using the uncertainties specified above to estimate probability distributions of the fit coefficients.

3.4 Measuring silk radii

Silk size was measured optically by measuring the separation of the diffraction fringes observed under parallel-polarized illumination with a wavelength of 546 nm and comparing them to theory [13]. Here, the silk size is quantified as the radii of the silk cylinders, which are assumed to be identical. This method yielded a radius measurement of 0.740 ± 0.055 μm for the *Plebs eburnus* silk and 1.09 ± 0.06 μm for the *Argiope keyserlingi* silk. This is an improvement in precision over conventional microscopy. The ability to measure silk size radius *in situ*, with high precision, is advantageous in terms of consistency and simplifying the experimental procedure, as silks had a tendency to break under electron microscopy.

Note that the presence of transverse optical structure does affect this measurement procedure. It can be seen from previous work, however, that radii measurements of *Argiope keyserlingi* silks were in good agreement with SEM data, suggesting that transverse optical structure, if present, is not sufficient to affect the uncertainty of these measurements.

4 Results

4.1 Homogeneous silks

Here, silks are first analyzed assuming them to be homogeneous, with the intent of using these results to establish, by contradiction with independent measurements of spider silks' optical absorption [5, 14], that silks possess transverse optical structure.

Measured principal real refractive indices (n_p, n_s) and imaginary refractive indices (κ) of a *Plebs eburnus* dragline silk and an *Argiope keyserlingi* dragline silk are shown in Figure 3. An analysis of the *P. eburnus* silk estimated these imaginary refractive index components to range from $(4.5 \pm 0.7) \times 10^{-4}$ at 450 nm to $(1.0 \pm 1.1) \times 10^{-4}$ at 589 nm. At 589 nm, it is reasonable to suppose that κ cannot be negative (implying optical gain); hence, $(1.0 \pm 1.1) \times 10^{-4}$ implies only an upper bound of 2.1×10^{-4}. For the *A. keyserlingi* silk, the imaginary refractive index component was estimated to range from $(9.3 \pm 1.0) \times 10^{-4}$ at 450 nm to $(4.5 \pm 0.8) \times 10^{-4}$ at 546 nm.

The corresponding optical absorption as a function of wavelength for these imaginary refractive index estimates are shown in Figure 4. Comparison of these estimates with

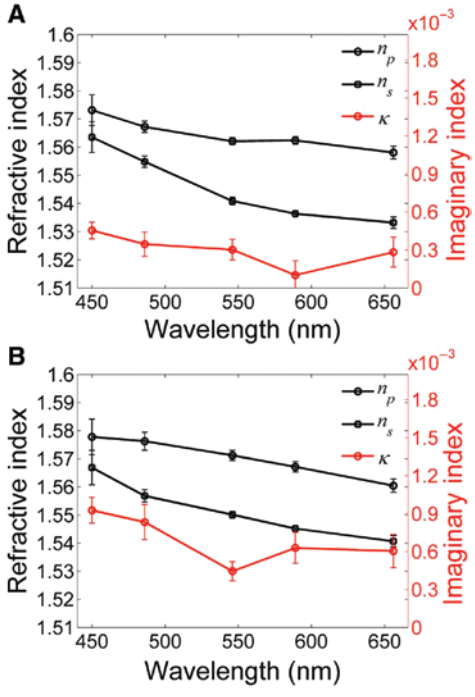

Figure 3: Measured principal real refractive indices, n_p and n_s, and predicted imaginary refractive index, κ, of (A) a *Plebs eburnus* dragline silk and (B) an *Argiope keyserlingi* dragline silk, assuming the silks to be homogeneous. Real refractive indices are marked in black (where $n_p > n_s$), and imaginary refractive indices are marked in red.

those of Huby et al. (1.0 ± 0.4 dB/mm for *Nephila clavipes* dragline silk at 633 nm [5]) and Tow et al. (0.2 ± 0.1 dB/mm for *Nephila edulis* dragline silk at 633 nm [14]) demonstrates that the estimated imaginary refractive indices are highly implausible. Therefore, it can be concluded with confidence that the assumption that the silks are optically homogenous is false and that they do, in fact, possess transverse optical structure.

4.2 Silks with transverse optical structure

The reason the method outlined in Section 2 overestimates the apparent absorption of homogeneous double cylinders is because the (real) refractive index mismatch present internally within each cylinder of the double-cylinder silk generates excess contrast, most evident in the calculation of C_0. The excess contrast was calculated as the error term ΔC_0, which is obtained using a "known" absorption. With some assumptions, the excess contrast can be used to infer aspects of the transverse optical structure of the silk double cylinders.

A uniform-layered double cylinder with inner radius, a_{in}, and internal refractive index contrast, Δn_{in}, can be modeled at an incident polarization orientation of θ_0, as a homogeneous double cylinder with cylinder axes spaced by $2a$ when the outer layer is refractive-index matched with its surrounds. Here, the following empirical formula was found to be accurate for estimating Δn_{in} from the scattering theory, provided this refractive index contrast does not have a strong polarization dependence;

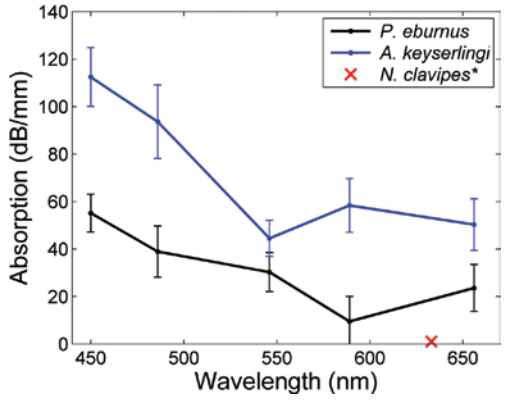

Figure 4: Estimated optical absorption of the *Plebs eburnus* dragline silk (black curve) and the *Argiope keyserlingi* dragline silk (blue curve), assuming no transverse optical structure. Absorption of *Nephila clavipes* dragline silk (red cross) measured by Huby et al. is shown for comparison [5]. The large disparity between estimates and independently measured values is strong evidence for the existence of transverse optical structure within the spider silks.

$$\Delta n_{in} \approx \frac{1}{26} \frac{\Delta C_0}{a_{in}^2} \tag{22}$$

where a_{in} is in μm. Setting a_{in} to be consistent with outer layer thicknesses observed with TEM (100 nm for *Plebs eburnus* dragline, 50 nm for *Argiope keyserlingi* dragline [8], yielding $a_{in} = 0.64$ μm and 1.04 μm, respectively), Δn_{in} was estimated to be $(1.6 \pm 0.2) \times 10^{-4}$ at 589 nm and $(3.6 \pm 0.3) \times 10^{-4}$ at 656 nm for the *P. eburnus* dragline, and $(5.5 \pm 0.5) \times 10^{-4}$ at 589 nm and $(5.1 \pm 0.4) \times 10^{-4}$ at 656 nm for the *A. keyerlingi* dragline. An absorption of 1.0 dB/mm was assumed for both silks; however, it should be noted that the influence of this absorption was minimal. Note that there is currently insufficient evidence to formulate an estimate for the uncertainty of a_{in}; however, the consequent uncertainty in Δn_{in} based on any given uncertainty of a_{in} can be worked out from Eq. (22).

This contrast in refractive index is indicative of a change in either the density or the mean polarizability of the silk over its cross-section. The relationship between density and refractive index is generally summarized by the Lorentz-Lorenz formula;

$$\frac{n^2 - 1}{n^2 + 2} = \frac{4\pi}{3} \frac{\alpha}{M} N_A \rho, \tag{23}$$

where α is the mean polarizability, M is the molar weight, and N_A is the Avogadro's constant. Taking the density of spider silk to be 1.3 g/cm^3, the ratio α/M is calculated to be around $0.058/N_A$ at 589 nm, giving $\partial\rho/\partial n = 1.94$ g/cm^3 for the *Plebs eburnus* dragline. Assuming that the mean polarizability and molar weight remains constant, a refractive index change of 1.6×10^{-4} corresponds to a density change of about 0.31×10^{-3} g/cm^3. For the *Argiope keyserlingi* dragline, $\partial\rho/\partial n$ was computed to be 1.89 g/cm^3, giving a density change of 1.04×10^{-3} g/cm^3. We note that these values of $\partial\rho/\partial n$ are similar to values that have been measured for a broad range of optical materials [15, 16].

Transverse optical structure may also manifest as a graded refractive index contrast. An approximate formula for the peak refractive index contrast can be derived from Eq. (22) by assuming that the contribution to ΔC_0 from each infinitesimal layer is additive,

$$\Delta n_p = a^2 \frac{\Delta n_{in}}{2} \left(\int_0^a rP(r)dr \right)^{-1}, \tag{24}$$

where Δn_p is the peak refractive index contrast, and $P(r)$ is the radial shape of the refractive index profile, scaled to a maximum value of 1. For example, if the refractive index profile is Gaussian with standard deviation σ_a, then,

$$\Delta n_p = \frac{\Delta n_{in}}{2}\frac{a^2}{\sigma_a^2}\frac{1}{1-\exp(-a^2/2\sigma_a^2)}. \quad (25)$$

If σ_a is taken to be $a_{in}/2$ as an example (making a_{in} the $1/e^2$ width), then the peak refractive index contrast of the *Argiope keyserlingi* silk is estimated from the values quoted above to be $(1.93\pm0.17)\times10^{-3}$ and $(1.79\pm0.14)\times10^{-3}$ at 589 nm and 656 nm, respectively.

It should be re-emphasized that these values for Δn_p and Δn_{in} are for the specific estimates of a_{in}, and these values would change with any change in a_{in}. In the case of a step index change, the $1/a_{in}^2$ dependence of Eq. (22) means the predicted Δn_{in} would increase by a factor of 4 if a_{in} is halved.

Determining a_{in} optically may be possible if the dispersion of the silk material is accurately known. Contrast measurements made at different wavelengths would enable a_{in} to be narrowed down to a single consistent value. Accurate measurement of spider silk dispersion and optical measurement of a_{in} are topics of future work.

5 Conclusion

We have investigated the transverse optical structure of *Plebs eburnus* and *Argiope keyserlingi* dragline spider silks using an inverse-scattering approach, facilitated through quantitative bright-field microscopy. Using the incident linear polarization to tune the refractive index matching between the birefringent silks and immersion liquid, it was observed that the image contrast was much higher than expected for homogeneous silks with an optical absorption around 1 dB/mm. We conclude on this basis that the silks possess transverse optical structure.

This excess contrast was used to estimate the internal refractive index contrasts, Δn_{in}, between the outer layer of the silks and silk core in each cylinder of the double-cylinder arrangement (which were assumed to be identical). Here, Δn_{in} was estimated to be $(1.6\pm0.2)\times10^{-4}$ for *Plebs eburnus* dragline silk with a uniform 100-nm-thick outer layer and $(5.5\pm0.5)\times10^{-4}$ for *Argiope keyserlingi* dragline silk with an outer layer thickness of 50 nm, both at a wavelength of 589 nm. This led to an estimated density contrast of 0.31×10^{-3} g/cm^3 and 1.0×10^{-3} g/cm^3 for the *P. eburnus* and *A. keyserlingi* draglines, respectively, assuming no changes to the mean polarizability. The method successfully differentiates these small differences, and this is the first estimate of the refractive index contrast between the outer layer and core of spider silks. Assuming different characteristics in the optical structure, such as different outer layer thicknesses and/or graded index profiles, changes these estimates.

Insights gained into the optical structure of spider silk using this technique will contribute to the eventual understanding of guided-mode behavior within the silk micro-fibers and how they evanescently interact with the surrounding medium. This understanding will be important for the use of spider silks in sensing applications moving forward.

It is also worth highlighting that the procedure described herein can be applied to optical micro-structures that have a cross-section that is invariant along their length. All this requires appropriate modification in the functions f_i, describing the scattered field profile. Similarly, the functions F_i can be modified to account for different illumination and imaging conditions.

Acknowledgments: This research was supported by the Australian Research Council (ARC) Discovery Project Grant DP130102674 and Macquarie University. The authors thank Professor Mariella Herberstein, Department of Biological Sciences, Macquarie University, for expert advice on spider biology and for access to webs from her laboratory.

References

[1] Gosline JM, Denny MW, DeMont ME. Spider silk as rubber. Nature 1984;309:551–2.
[2] Shao Z, Vollrath F. The effect of solvents on the contraction and mechanical properties of spider silk. Polymer 1999;40:1799–806.
[3] Demura M, Asakura T, Nakamura E, Tamura H. Immobilization of peroxidase with a Bombyx mori silk fibroin membrane and its application to biophotosensors. J Biotechnol 1989;10:113–9.
[4] Lawrence BD, Cronin-Golomb M, Georgakoudi I, Kaplan DL, Omenetto FG. Bioactive silk protein biomaterial systems for optical devices. Biomacromolecules 2008;9:1214–20.
[5] Huby N, Vié V, Renault A, Beaufils S, Lefèvre T. Native spider silk as a biological optical fiber. Appl Phys Lett 2013;102:123702.
[6] Gosline JM, Guerette PA, Ortlepp CS, Savage KN. The mechanical design of spider silks: from fibroin sequence to mechanical function. J Exp Biol 1999;202:3295–303.
[7] Sponner A, Unger E, Grosse F, Weisshart K. Differential polymerization of the two main protein components of dragline silk during fibre spinning. Nat Mater 2005;4:772–5.
[8] Naidoo N, Little DJ, Birch D, Herberstein ME, Kane DM. Optical surface profilometry and AFM of spider web silks. In: Conference Proceedings of the 2012 International Conference on Nanoscience and Nanotechnology, B. Griffin, L. Faraone and M. Martynuik, eds. IEEE, 2012, paper 714.
[9] Little DJ, Kane DM. Hybrid immersion-polarization method for measuring birefringence applied to spider silks. Opt Lett 2011;36:4098–100.

[10] Bohren CF, Huffman DR. Absorption and scattering of light by small particles. New York, USA: Wiley, 1998, Chap. 8.
[11] Yousif HA, Köhler S. Scattering by two penetrable cylinders at oblique incidence I The analytical solution. J Opt Soc Am A 1988;5:1085–96.
[12] Hartmann J. A simple interpolation formula for the prismatic spectrum. Astrophys J 1898;8:218–22.
[13] Little DJ, Kane DM. Subdiffraction-limited radius measurements of microcylinders using conventional bright-field optical microscopy. Opt Lett 2014;39:5196–9.
[14] Tow KH, Chow DM, Vollrath F, Dicaire I, Gheysens T, Thévenaz L. Spider silk: a novel optical fibre for biochemical sensing. Proc. SPIE 2015;9634:96347D-1.
[15] Kakiuchida H, Saito K, Ikushima AJ. Refractive index, density and polarizability of silica glass with various fictive temperatures. Jpn J Appl Phys 2004;43:L743.
[16] Kurtz Jr SS, Camin DL, Thompson AR. Refractive index-density slope associated with volume change on mixing. J Chem Eng Data 1965;10:335–9.